Transactions, SMiRT-26
Berlin/Potsdam, Germany, July 10-15, 2022
Division V

SEISMIC RESISTANCE EVALUATION OF REINFORCED CONCRETE STRUCTURES WITH COMPLEX PLANAR SHAPES

Takaki Tojo[1], Noriki Nakai[2], Kazuhiro Kosaka[2], Kosuke Motoki[2], Hiroki Yamada[2], Takuya Suzuki[1], Akinobu Takada[1], Soshi Nakamura[1] and Naoto Yabushita[1]

[1] Takenaka Corporation, Tokyo, Japan (toujou.takaki@takenaka.co.jp)
[2] The Kansai Electric Power Co., Inc., Osaka, Japan

ABSTRACT

Concrete buildings in nuclear power plant (NPP) are often box-frame structures with reinforced concrete (RC) shear walls. Generally, these structures are designed in accordance with the NPP seismic design technical provision. However, the applicability of the provision to complex box frame structures for dynamic analysis is still unclear. In this study, the seismic response of NPP buildings with irregular shaped RC shear walls was evaluated using a finite element (FE) model. Moreover, its seismic response was compared with that of a multi degree of freedom system applying the current seismic technical provision. The results confirmed that even when the current seismic technical provision was applied to complicated box frame structures, the response evaluation is equivalent or conservative to the FE model.

INTRODUCTION

Buildings in nuclear power plants (NPP) often have irregularly shaped box frame structures with reinforced concrete (RC) shear walls depending on the layout of nuclear equipment. In Japan, generally, these structures are designed in accordance with the NPP seismic design technical provision (herein referred to as the JEAC (2015)) issued by Japan Electric Association (2015) assuming a box-shaped or cylindrical structure. However, the applicability of the provision to box frame structures with complex shapes such as internal concrete (I/C) structures is still unclear. Previously, the authors focused on an I/C structure within a standard pressurized water type reactor (PWR) building and confirmed that the load-deformation relationship evaluated by the current provision of JEAC (2015) was generally appropriate compared to that of static stress analysis using non-linear (NL) finite element (FE) model (Tojo et al. (2020)). However, the applicability of the provision has not been confirmed for dynamic analysis.

In this study, we evaluate its realistic dynamic response characteristics by conducting seismic response analyses using the NL FE model. Furthermore, the applicability of the provision for evaluating dynamic responses for irregularly shaped structures is confirmed by comparing responses of a multi degree of freedom (MDOF) system applied the JEAC (2015) with those of FE model. First, analysis overview is explained. Then, result of NL analysis is shown. Finally, conclusions and future works are dicussed.

ANALYSIS OVERVIEW

Overview of FE Model

An overview of the analysis model used in this study is shown in Figure 1(a), and a plan view of stories 1 and 3 is shown in Figure 1(b). This model is same as the that of Tojo et al. (2020), which can be referred

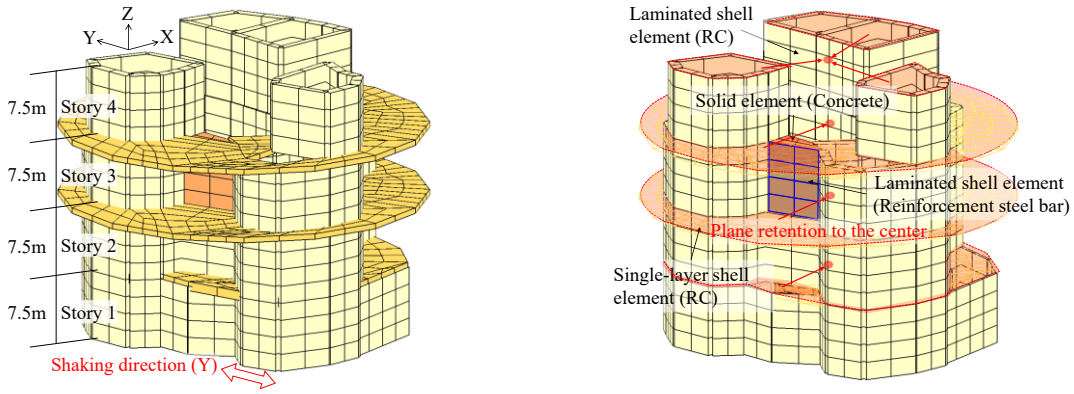

(a) Bird's-eye view

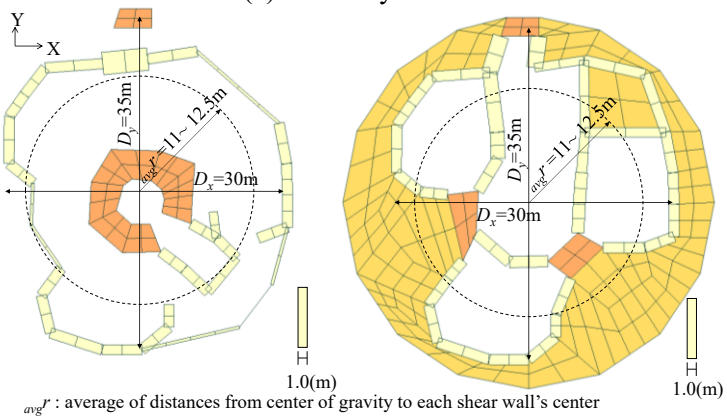

(b) Plan view (Left: Story 1, Right: Story 3)

Figure 1. Configuration of the I/C structure modelled by FE method.

Table 1: Specifications of FE model.

Concrete					Rebar	
Compressive strength f_c (N/mm ^{2})	Tensile strength f_t (N/mm ^{2})	Young's modulus E_c (N/mm ^{2})	Poisson's ratio ν	Density ρ (t/m ^{3})	yield stress $_s\sigma_y$ (N/mm ^{2})	Young's modulus E_s (N/mm ^{2})
24.5	1.88	22,800	0.2	2.4	345	205,000

to for details. Outline of the model is as follows. The building model has four stories, and each story's height is 7.5 m. Regarding the plane arrangement of the seismic shear wall, both the maximum distances D_x and D_y between seismic shear walls are apprximately 30 m and 35 m, respectively, in X and Y directions in the figure. The average distance $_{avg}r$ from the model centre to the gravity point for each seismic shear wall is approximately from 11 to 12.5 m in each floor. The wall whose with approximately 0.3–2 m thickness is modelled by the laminated shell element. Other large cross-sections and irregularly shaped continuous walls are modelled by solid elements. Each element for the shear wall is elasto-plastic material; however, this slab is an elastic single-layer shell element. In this study, each floor is assumed to be plane retention to the centre to focus on the effect of the irregularly arranged seismic shear walls on the response.

The specifications of concrete and reinforcement steel bar are shown in Table 1. The compressive strength f_c of concrete is 24.5 (N/mm^2) for both seismic shear walls and slabs. The tensile strength f_t is

obtained from Eq. (1) according to the structural calculation standard of RC (Architectural Instituted of Japan (2010)).

$$f_t = 0.38\sqrt{f_c} \tag{1}$$

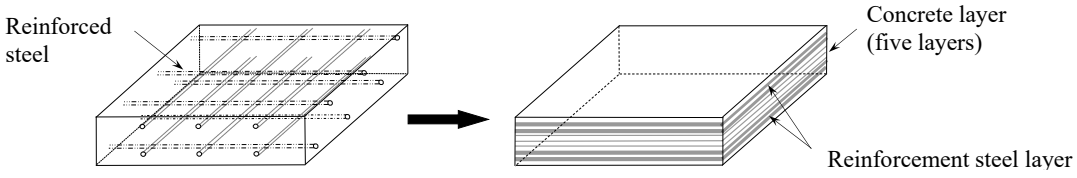

Figure 2. Laminated shell elements.

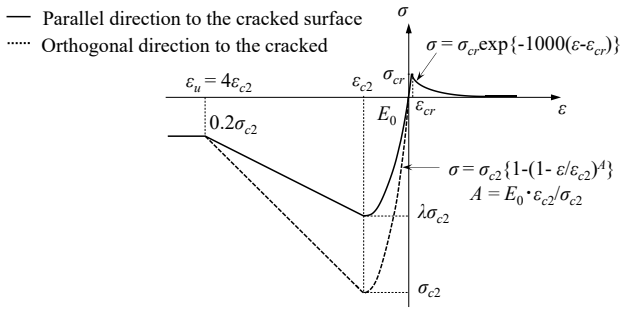

Figure 3. Relationship between the uniaxial stress and strain of concrete after cracking.

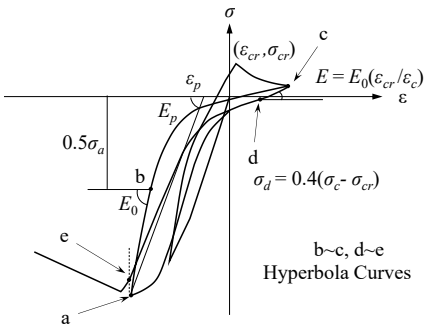

Figure 4. Hysteresis characteristics of the cracked surface.

Elasto-plastic Characteristics of FE Model

In this analysis, laminated shell and solid elements are used to represent the elasto-plastic properties of the RC walls. These elements were subjected to simulation analysis to test restoring force characteristics, such as RC seismic shear walls. It was confirmed that the load-deformation relation from the test could be approximately reproduced by the analysis (e.g., Akita et al. (2013), Kudo et al. (2018)).

The elasto-plastic properties of Laminated shell elements are shown in Figure 2 to Figure 4. For these elements, the elasto-plasticity of the material is considered with respect to the in-plane stress-strain relationship. The out-of-plane shear deformation component is treated as elastic. Based on the previous paper (Akita et al. (2013)), outline of each elasto-plastic properties of laminated shell elements is as follows.

- A trilinear elasto-plastic constitutive relationship is used for uncracked concrete.
- The yield surface is used for the cracking and compression-side yield conditions.
- The relationship between stress and strain after cracking is evaluated as two axial springs, one in the direction of the crack and another parallel to the crack direction (Figure 3).
- On the crack surface, shear is transferred by the engagement of the friction force between the concrete and aggregate and the reinforcement dowel effect. This shear transfer force is evaluated as a decreasing function of the strain orthogonal to the crack.
- After cracking, the concrete exhibits the hysteresis characteristics represented by the hyperbolic curves shown in Figure 4.
- The relationship between reinforced steel's stress and strain exhibits bilinear hysteresis characteristics (detail is shown in following solid elements part).

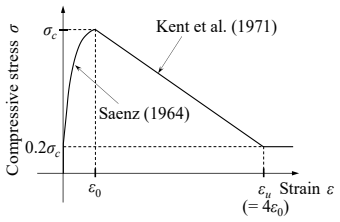

Figure 5. Compression characteristics of concrete.

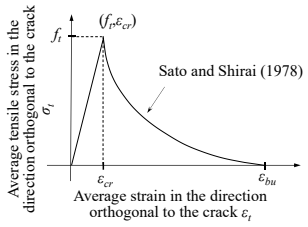

Figure 6. Tensile characteristics of concrete.

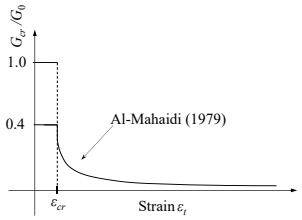

Figure 7. Shear transfer characteristics of concrete.

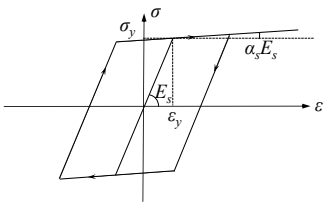

Figure 8. Hysteresis characteristics of reinforcement steel bar.

The elasto-plastic properties of solid elements are summarized below.

- The constitutive law of Noguchi et al. (2009) is used for the hysteretic characteristics of concrete.
- Regarding the stress-strain relationship, the compressive side rise region is described by the equation of Saenz (1964), and the softening region is a straight line adopted by Kent et al. (1971) (see Figure 5).
- The tensile side is made to be linear up to the crack generation point, beyond which the tension stiffening characteristic is modelled as per Sato and Shirai (1978) (see Figure 6).
- The model of Al-Mahaidi (1979) is applied to the shear transfer characteristics after cracking (see Figure 7).
- Reinforcement steel bars are laminated shell elements with bilinear restoring force characteristics as uniaxial material for the reinforcement arrangement direction (see Figure 8). The second gradient is 1/1000 of the initial stiffness. Complete adhesion is assumed between reinforcement and concrete.

MDOF System with Restoring Force Characteristics based on Current Design Provision

The stiffness, strength evaluation method, and specifications of the MDOF system based on the current design provision (JEAC (2015)) compared with FE model are shown below. The modeling is performed in the Y direction of Figure 1 (a). Although omitted in this paper, it was confirmed that the same tendency was obtained in the X and Y directions for the response results described later.

The MDOF system is modelled by beam element having bending and shear deformation characteristics. The specifications of the MDOF system are shown in Table 2. The initial stiffness was calculated separately for shear and bending stiffness based on the strain energy method (e.g. Kitamura (2002)) using the FE model described above. For the lumped mass of each floor, calculated from FE model assuming that the dominant thickness was half of each story. The displacement distribution in the horizontal direction when bending and shear deformation separated adopts the primary mode vibration distribution obtained from the eigenvalue analysis of the FE model. The initial rigidity is calculated from the separation method using the relation between displacement and force.

The restoring force characteristics and hysteresis characteristics in the MDOF system are estimated based on JEAC (2015). The restoring force characteristics for the set shear and bending deformation are

shown in Table 3 and Table 4, respectively. Each yield force Q_i was calculated by multiplying the shear stress τ_i obtained from JEAC (2015) by the shear cross sectional area of Table 2. For both shear and bending deformation, the skeleton curve is assumed as a trilinear distribution, and the hysteresis characteristic is a maximum point oriented type for shear deformation and a degrading trilinear type for bending deformation. Where, the shear span ratio M/Qd at the time of setting the shear deformation characteristics was calculated using the maximum moment M and the maximum shear force Q obtained from the seismic response analysis under linear conditions in the FE model subjected to the seismic motion described later. The distance d between the tensile and compressive flanges is set to 25 m.

Table 2: Specifications of MDOF system.

Story	Weight		Axial section area A	Shear section area A_s (Y)		Moment of inertia of area I (R_X)
	M	ΣM				
	(kN)	(kN)	(m^2)	(m^2)	A_s/A	(m^4)
4	9,850	9,850	112	53	0.47	10,300
3	37,010	46,860	206	129	0.63	19,500
2	50,170	97,030	230	149	0.65	14,100
1	54,550	151,580	187	108	0.58	19,200

Table 3: Restoring force characteristics of shear deformation (Q-γ) in the Ydirection.

Story	1st yield point		2nd yield point		3rd yield point	
	Q_1 (MN)	γ_1 ($\times 10^{-3}$)	Q_2 (MN)	γ_2 ($\times 10^{-3}$)	Q_3 (MN)	γ_3 ($\times 10^{-3}$)
4	83.1	0.166	112	0.498	302	4.00
3	212	0.173	286	0.519	714	4.00
2	258	0.182	348	0.547	804	4.00
1	204	0.200	275	0.599	586	4.00

Table 4: Restoring force characteristics of bending deformation (M-ϕ) in the Ydirection.

Story	1st yield point		2nd yield point		3rd yield point	
	M_1 (MN·m)	ϕ_1 ($\times 10^{-3}$/m)	M_2 (MN·m)	ϕ_2 ($\times 10^{-3}$/m)	M_3 (MN·m)	ϕ_3 ($\times 10^{-3}$/m)
4	1,200	0.00511	3,340	0.0689	5,990	0.915
3	2,240	0.00503	8,330	0.0660	14,600	0.662
2	2,430	0.00755	9,630	0.0702	16,800	0.596
1	2,460	0.00563	9,730	0.0695	16,400	0.452

Analysis Conditions and Seismic Input Motion

Time history response analysis was conducted using FE model and MDOF system as shown above. The

analysis time step was 0.002 s, and the Newmark-β method (β = 0.25) was used for the time integration. The Newton-Raphson method was used for the convergence calculation. The damping model was adopted as Rayleigh type (reference frequencies f_1 and f_2 were set to 10.2 and 27.4 Hz, respectively) for FE model, the strain energy proportional type for the MDOF system, and damping ratio h was set to 4.85% in common.

Acceleration time history and acceleration response spectrum of seismic input motion (maximum acceleration of 10 m/s^2) are shown in Figure 9. Three cases (Acc. 10, Acc. 20, Acc. 30) standardized at maximum accelerations of 10, 20, and 30 m/s ^{2} were carried out with reference to the seismic motion of large amplitude level required in the probabilistic risk assessment (Atomic Energy Society of Japan Standard (2015)). They are shown as input in the Y direction of Figure 1.

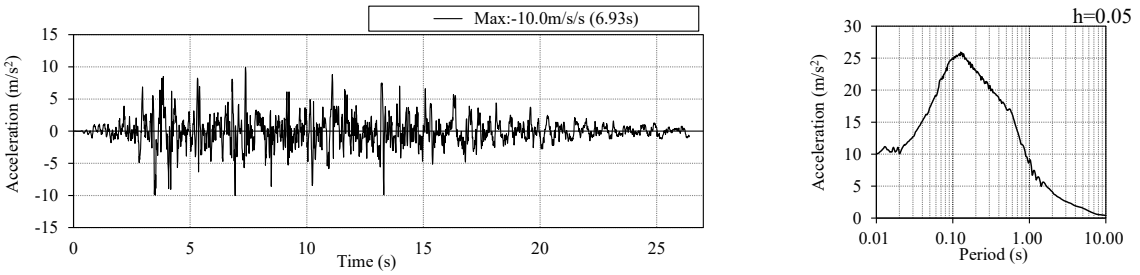

(a) Acceleration time history (b) Acceleration response spectrum

Figure 9. Input seismic motion.

RESULT OF NON-LINEAR ANALYSIS

By comparing the dynamic analysis results of the FE model and those of the MDOF system subjected to seismic motions with different amplitude levels, the applicability of the MDOF system based on the current design provision in relatively weak to strong nonlinear conditions is examined. Moreover, the effect of the irregularly arranged seismic walls on the response characteristics is examined.

Comparison of Load-Deformation Relationships between FE Model and MDOF System

The comparison of the story shear force-shear strain (Q-γ) relationship between first- and second-story of the FE model and the MDOF system is shown in Figure 10. The comparison of the overturning moment-curvature (M-ϕ) relationship of first story, which has a relatively large plasticity, for each model is shown inFigure 11. The story shear force, overturning moment, shear strain, and curvature of the FE model were obtained from Eq. (2) to Eq. (7), respectively. The overturning moment in Figure 11 is the average of the values at the top and bottom of each story, and the curvature is the value at the middle of the story. For reference, the skeleton curve set in the MDOF system is described in each figure.

$$Q_i = 0.5\left(\sum P_{ij}^t + \sum P_{ij}^b\right) \tag{2}$$

$$M_i^s = \sum N_{ij}^s \cdot l_{ij}^s + R_{ij}^s \ (s{=}t \text{ or } b) \tag{3}$$

$$\delta_{S_i} = \delta_{T_i} - \delta_{M_i} \tag{4}$$

$$\delta_{M_i} = 0.5H_i(\theta_i^t + \theta_i^b) \tag{5}$$

$$\gamma_i = \delta_{S_i}/H_i \tag{6}$$

$$\phi_i = (\theta_i^t + \theta_i^b)/H_i \tag{7}$$

where i indicates story number, j indicates node number, and t and b indicate the top and bottom of the

story, respectively. P_{ij}, N_{ij}, R_{ij} are the equivalent nodal forces (shear direction, axial direction and rocking direction, respectively) at node j and layer i, and l_{ij} is the arm length from the center point to node j. δ_{Si}, δ_{Ti}, and δ_{Mi} show the shear displacement, total displacement, and rocking displacement between stories in Story i, respectively. H_i is the story height.

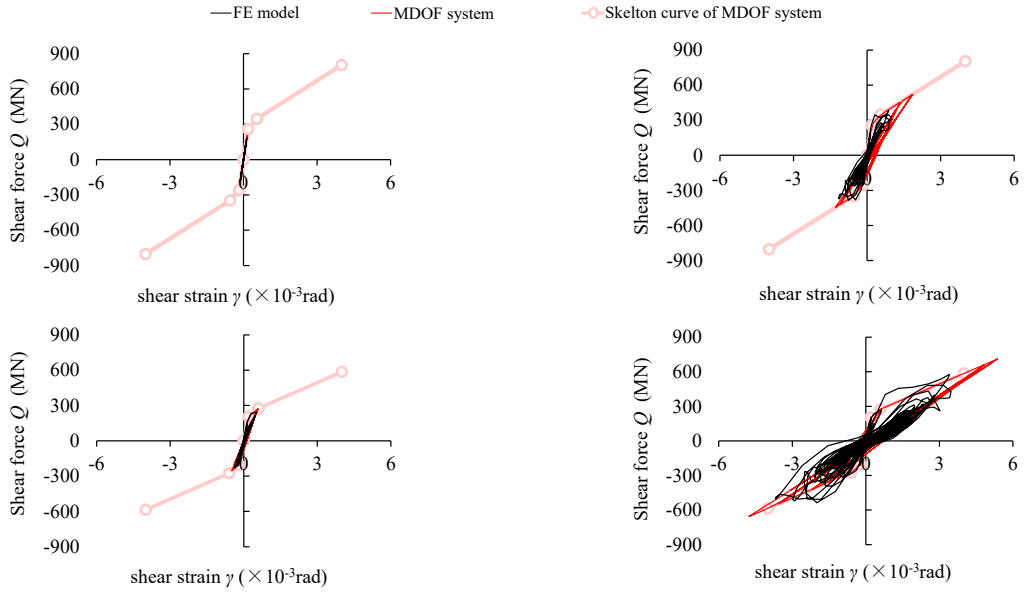

(a) Case: Acc. 10 (b) Case: Acc. 30

Figure 10. Relations between shear force Q and shear strain γ (Top: Story 2, Bottom: Story 1).

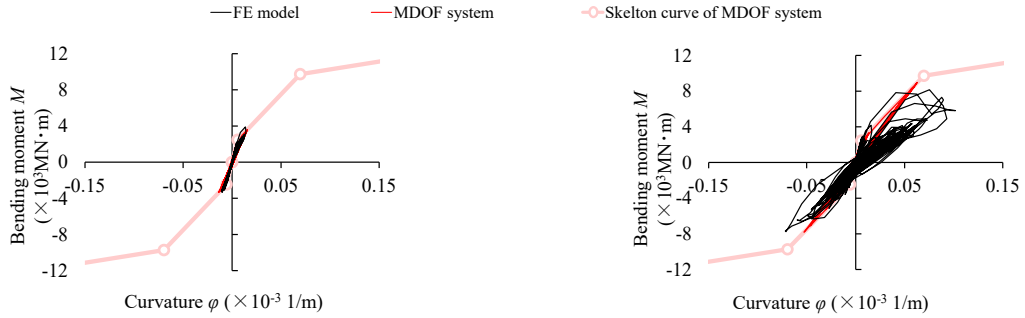

(a) Case: Acc. 10 (b) Case: Acc. 30

Figure 11. Relations between bending moment M and curvature ϕ for Story 1.

The Q-γ relationship in Figure 10(a) shows that the initial stiffness, restoring force characteristic after the first yield point, and hysteresis characteristic of Acc. 10, which has a relatively small amplitude level, correspond to each other. As shown in Figure 10(b) in the case of Acc. 30 with a large amplitude level, both the load and deformation of the MDOF system are larger than those of the FE model. For first-story , which has a relatively large plasticity, the story shear force between the second and third yield points of first-story indicates that the FE model is larger than the MDOF system.

Regarding the M-ϕ relationship in Figure 11(a), for the Acc. 10, both restoring force characteristics including initial stiffness and hysteresis characteristics generally correspond to each other with similar tendency to the Q-γ relationship. In Acc. 30 shown in Figure 11(b), the maximum moment approximately

corresponds to the FE model and the MDOF system. The hysteresis loop of the FE model is larger and more complicated than that of the MDOF system for first-story. The MDOF system conservatively evaluates energy consumption associated with plasticity. These relationships also correspond to the results of the maximum response value distribution described later (shown in Figure 12). However, in the FE model, the shear deformation and bending deformation components are separated using Eq. (4) − (7). Therefore, the separation accuracy of these deformations may be lowered when the nonlinearity is large.

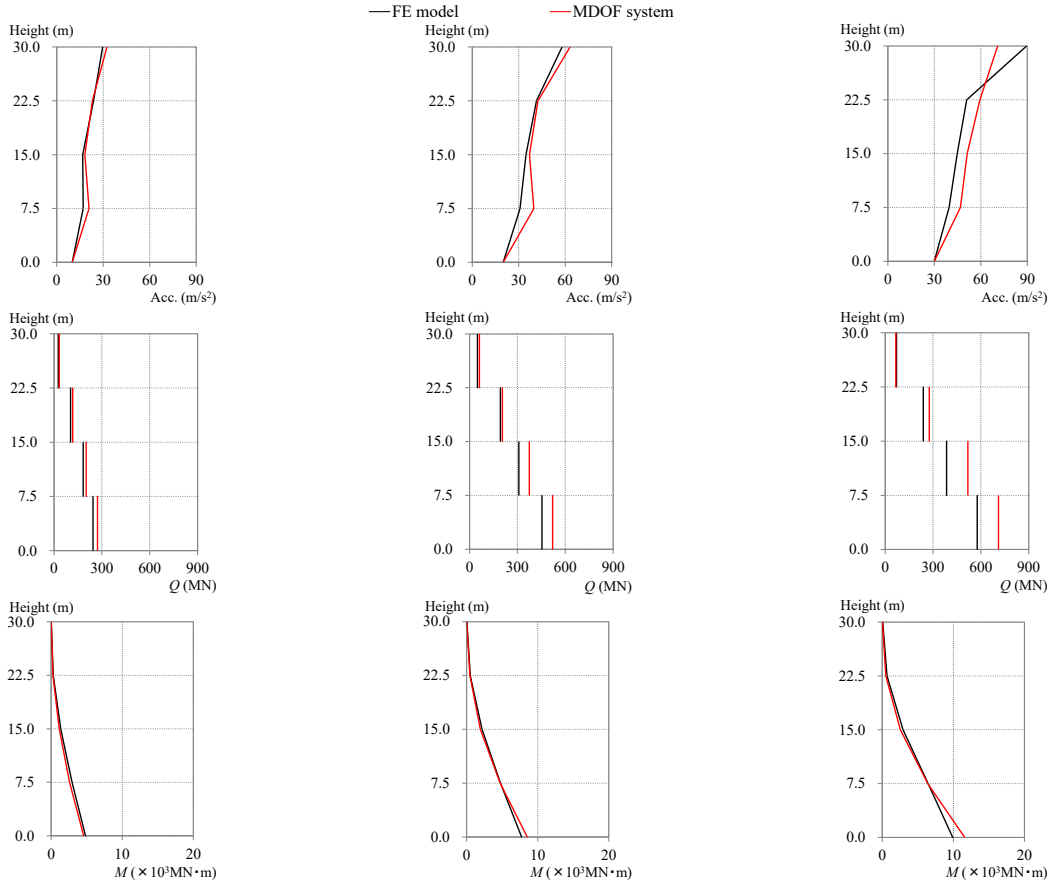

(a) Case: Acc. 10 (b) Case: Acc. 20 (c) Case: Acc. 30

Figure 12. Maximum response distribution (Top: Acc. Middle: Shear force, Bottom: Bending moment).

Comparison of Maximum Responses between FE Model and MDOF System

The maximum response value distributions of the FE model and the MDOF system from Acc. 10 to Acc. 30 are compared with those in Figure 12(a) to (c). From the top of the figure, acceleration, story shear force, and overturning moment are arranged in this order.

In Figure 12(a) - (c), for Acc. 10 where the amplitude level is small, the FE model and the MDOF system almost correspond well, and the maximum difference is less than 10–15 %. In Acc. 30, the response of the MDOF system is approximately from 20 to 25% larger than that of the FE model in the lower stories. The difference in terms of the amplitude level is comparatively small for acceleration and overturning moment except for the acceleration response of the top. In both the FE model and MDOF system, the response values of the forth-story are assumed to be within the elastic range, so it is assumed that the

difference of acceleration response at the top depend on the changes of vibration mode distribution according to the plasticization of the lower stories.

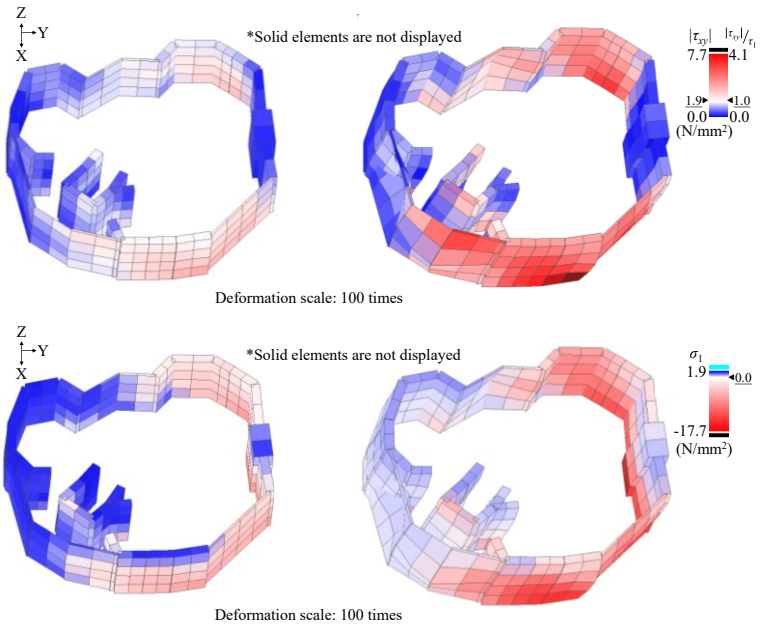

(a) Time when the second yield shear force reached (2.96 s)

(b) Time when the maximum shear force reached (3.63 s)

Figure 13. In-plane stress contour of Story 1 in Acc.30
(Top: shear stress τ_{xy}, Bottom: maximum principal stress σ_1).

Comparison of Stress Contour for FE Model in the Case of Large Amplitude Level (Acc.30)

In the case of Acc. 30 with the largest amplitude level, the difference in response between the FE model and the MDOF system tended to be larger, especially with respect to the story shear force. To examine this factor, focusing on the case of Acc. 30, the stress state of the laminated shell elements are confirmed at a time (2.96 s) when the first-story shear force of the FE model reaches approximately the second yield point (Q_2 in Table 3) of the MDOF system , and at a time (3.63 s) when the shear force reaches its maximum.

Figure 13 shows the contours of the shear stress of the laminated shell elements (top) and the maximum principal stress (bottom) at each time. In the legend of the former, the maximum value is aligned with the element maximum value (7.7 N/mm^2) at 3.63 s, and the ratio from the first yield point shear stress (1.9 N/mm^2) is also indicated on the right side of the legend. In the legend of the latter, the compressive side (negative side) is the element maximum value (-17.7 N/mm^2) in 3.63 s, and the tensile strength (1.9 N/mm^2) obtained from the Eq. (1) is used for the tensile side (positive side).

In terms of shear stress, the bearing stress in the wall arranged in excitation parallel or in oblique direction tends to increase with the progress of the yield of the surrounding seismic shear wall at 3.63 s although their stress was comparatively small at 2.96 s. Regarding principal stress, it was found that the element in which tensile stress was generated at 2.96 s hardly bears tensile force at 3.63 s due to tensile yield of concrete. In the FE model, the shear or bending (vertical) load area changes with the redistribution of stress. Regarding the Q-γ relationship of the MDOF system in Table 3, since the shear cross sectional aera is invariant regardless of the degree of plasticity, it is considered that the plasticity progresses easily compared with the FE model. Therefore large story shear force occurs easily in the MDOF system.

CONCLUSIONS AND FUTURE CHALLENGES

1) The response of MDOF system adopted the relationship between load and deformation based on JEAC (2015) generally corresponds well to that obtained using the FE model dynamic analyses. In the FE model, the yield strength tends to be relatively large compared with that based on JEAC (2015) due to the influence of stress reallocation for the obliquely arranged RC shear walls when the progress of plasticization increases. These tendencies are similar to the comparative results on the maximum yield strength obtained by static stress analysis (Tojo et al. (2020)), and similar tendencies are obtained in dynamic analysis.
2) In terms of the maximum response value of dynamic response analyses, the MDOF system tends to respond similar the FE model when the degree of plasticity is relatively small. In contrast, when the degree of plasticity increases according to the large amplitude level, the MDOF system's response diverges from that of the FE model, and evaluation of the MDOF system is relatively conservative. In the FE model, the shear stress is redistributed to shear walls arranged in parallel or diagonally according to the increase in deformation, whereas, in the MDOF system, the stress burden range does not depend on the degree of plasticization. Therefore, the plasticization tends to proceed in the MDOF system.

Since this study assumes the input in the single horizontal direction, the effect evaluation considering three-dimensional response property in the multidirectional input is planned as a future work.

REFERENCES

Architectural institute of Japan. (2010). *AIJ Standard for Structural Calculation of Reinforced Concrete Structures revised 2010*, 73

Akita, S., Miake, M., Nakamura, N., Suzuki, T., Kinosita, T. and Nakano, T. (2013). "Study of damage index of reinforced concrete shear wallbased on consumed energy using 3D FEM," *The AIJ Journal of Technology and Design*, Architectural Institute of Japan, Tokyo, Japan, vol. 19, No. 41, 77-82

Al-Mahaidi, R.S.H. (1979). "Nonlinear Finite Element Analysis of Reinforced Concrete Deep Members," Report 79-1, Department of Structural Engineering, Cornell University

Atomic Energy Society of Japan. (2015). *A Standard for Procedure of Seismic Probabilistic Risk Assessment for Nuclear Power Plants: 2015(AESJ-SC-P006E：2015)*

Japan Electric Association. (2015). *Nuclear power plant seismic design technical provision, JEAC4601-2015*, 187-198

Kent, D.C. and Park, R. (1971). "Flexural members with confined concrete," *Journal of the Structural Division*, American Society of Civil Engineers, Vol. 97, No. ST7, 1969-1990

Kitamura, H. (2002). Seismic Response Analysis Methods for Performance Based Design, 75-82

Kudo, W., Tojo, T., Yamamoto, S., Suzuki, T., Tsunasima, N., Takada, A. and Igaki, R. (2018). "Seismic resistance evaluation of reinforced concrete structures using the 3D finite element method Part 1,2." *Summaries of Technical Papers of Annual Meeting*, Architectural Institute of Japan, Structure-Ⅱ, 1179-1182

Noguchi, H., Kashiwazaki, T. and Miura, K. (2009). "Finite element analysis of reinforced concrete joints subjected to multi-axial loading," *Thomas T.C. Hsu Symposium*, ACI, vol. 265, 223-244

Saenz, L.P. (1964). "Discussion of Equation for the Stress-strain Curve of Concrete by Desayi and Krishnan," *Journal of the American Concrete Institute,* Vol. 61, 1229-1235

Sato, T. and Shirai, N. (1978). "Study on elasto-plastic behavior of reinforced concrete shear walls: Part 6 Inelastic analysis considering bond characteristics in tensile stress–strain curve." *Summaries of Technical Papers of Annual Meeting*, Architectural Institute of Japan, 1615-1616

Tojo, T., Tanaka, K., Yamamoto, S., Tsunashima, N., Suzuki, T., Takada, A. and Yabushita, N. (2020). "Evaluation of seismic performance for the complex structure of planar arrangement with reinforced concrete shear walls," *The AIJ Journal of Technology and Design*, Architectural Institute of Japan, vol. 26, No. 62, 91-96